Title: SARS-CoV-2 induces acute neurological signs while Calcitonin Gene-Related Peptide (CGRP) signaling blockade reduces interleukin 6 (IL-6) release and weight loss in mouse models.

Abbreviated title: SARS-CoV-2 induces acute neurological signs while CGRP signaling blockade reduces interleukin 6 (IL-6) release and weight loss

Authors: Shafaqat.M. Rahman [1,co], David W. Buchholz[2,co], Brian Imbiakha.[2,co], Mason.C. Jager[3], Justin Leach, [1], Raven.M. Osborn [1], Ann O. Birmingham [1], Stephen Dewhurst[1], Hector C. Aguilar [2,*] , and Anne E. Luebke, [1,*]

Affiliations:

[1]University of Rochester Medical Center, Departments of Biomedical Engineering, Neuroscience, Microbiology and Immunology, Rochester, NY, USA;

[2] Cornell University, Department of Microbiology and Immunology, College of Veterinary Medicine, Ithaca, NY, USA.

[3] Cornell University, Department of Population Medicine, College of Veterinary Medicine, Ithaca, NY, USA.

[co] Contributed equally

*Send correspondence to: Anne E. Luebke (aluebke@ur.rochester.edu) or Hector C. Aguilar (haguilar@cornell.edu)

Submitting author: Anne E. Luebke (aluebke@ur.rochester.edu)

Number of Pages: 29

Number of Figures: 6

Number of Tables: 0

Number of words for Abstract: 151

Number of words for Significance Statement: 102

Number of words for Introduction: 591

Number of words for Discussion: 361

Conflict of interest statement: The authors declare no competing financial interests.

Acknowledgments: This research is supported by a COVID-19 research supplement to NIH R01 DC017261 (AEL). We would also like to thank Dr. Ralph S. Baric (UNC) for the MA-10 SARS CoV-2 virus stock, the BSL3 facility and staff in the Center for Advanced Research Technologies at the University of Rochester, and the ABSL3 facility and staff at Cornell University. We would also like to thank Shruti Aryal for assisting with data analysis.

Abstract:

COVID-19 can result in neurological symptoms such as fever, headache, dizziness, and nausea. We evaluated whether the Calcitonin Gene-Related Peptide (CGRP) receptor antagonist, olcegepant, used in migraine treatment could mitigate acute neuroinflammatory and neurological responses to SARS-COV-2 infection. We infected wildtype C57BL/6J and 129/SvEv mice, and a 129 αCGRP-null mouse line with a mouse-adapted SARS-CoV-2 virus, and evaluated the effect of CGRP receptor antagonism on the outcome of that infection. We determined that CGRP receptor antagonism provided protection from permanent weight loss in older (>12 m) C57BL/6J and 129 SvEv mice. We also observed acute fever and motion-induced dizziness in all older mice, regardless of treatment. However, in both wildtype mouse lines, CGRP antagonism reduced acute interleukin 6 (IL-6) levels by half, with virtually no IL-6 release in mice lacking αCGRP. These findings suggest that blockage of CGRP signaling protects against acute IL-6 release and subsequent inflammatory events after SARS-CoV-2 infection.

Significance Statement:

COVID-19 can cause neurological symptoms such as fever, headache, dizziness, and nausea. However, such neurological symptoms of SARS-CoV-2 infection have not been assessed in mouse models. Here, we infected two commonly used wildtype mice lines (C57BL/6 and 129S) with mouse-adapted SARS-CoV-2 – and demonstrated neurological signs that including motion-related dizziness. Further, we show that CGRP signaling blockade can reduce IL-6 release and reverse long-term weight loss associated with SARS-CoV-2 infection, without rescuing either fever and/or dizziness. These findings suggest that CGRP signaling blockade can be protective in acute SARS-CoV-2 infections, and raise the possibility that it may also impact long-term outcomes of infection.

Introduction

Coronavirus disease (COVID-19) caused by severe acute respiratory syndrome CoV-2 (SARS-CoV-2) has caused a 3-year, ongoing, world pandemic [1]. There is a sound premise supporting testing CGRP-receptor antagonists such as olcegepant as a way to mitigate the neuroimmune consequences of SARS-CoV-2 infection [2]. While CGRP has pleotropic effects on the immune system, CGRP release occurs as a result of SARS-CoV-2 activation of the transient receptor potential (TRP) channels; and is implicated in COVID-19 neurological symptoms such as fever, headache, dizziness, nausea pain, and the subsequent release of interleukin 6 (IL-6) [3-5]. IL-6 is an important mediator of inflammation that is often elevated in severe COVID-19 infection, and may be involved in the hyperimmune response cascade (cytokine storm) and the polarization of T-cell responses [6, 7]. Headache, nausea, and dizziness are common neurological manifestations of COVID-19 infection [8-10], and in COVID-19 patients headache severity has been correlated with IL-6 levels [11]. However, there have been no studies on animal models investigating dizziness and fever after SARS-CoV-2 infection [12] .

Studies have shown that both SARS-CoV-1 (2002 outbreak) and SARS-CoV-2 (2019 outbreak) enter the body by binding to the angiotensin-converting enzyme 2 (ACE2) cell receptor [13, 14]. However, due to sequence and structural differences between mouse ACE2 and human ACE2, human SARS coronaviruses exhibit a species-restricted tropism and are inefficient at infecting wild-type mice. To overcome this obstacle, the Baric laboratory modified the clinical SARS-CoV-2/USA-WA1 variant to gain the ability to bind to the murine ACE2 receptor after serial passaging in mice, to generate the MA10-SARS-CoV-2 virus [15, 16]; we used this mouse-adapted virus in most of our study.

We first assessed both neurological symptoms of fever and dizziness/nausea in mouse models after infection with the MA10-SARS-CoV-2 virus. As a readout of the nausea-like state present

after SARS-CoV-2 infection, we examined hypothermic responses to provocative motion, as we have previously used to assess migraine nausea pain (Biorxiv doi.org/10.1101/2022.06.03.494762) and others have used to assess motion-sensitivity in transgenic mouse models [17]. Studies have demonstrated that provocative motion causes robust and prominent hypothermic responses in rats, humans, house musk shrews, and mice. These decreases in body temperature can represent a biomarker of a nausea-like state in laboratory animals as: i) temperature changes are provoked both by motion and by chemical emetic stimuli, ii) differential pharmacological sensitivity of these responses mirrors sensitivity in humans, iii) motion-induced hypothermia *precedes* emetic (vomiting) episodes, and iv) there is a clear parallel in hypothermic responses between animals and humans in underlying physiological mechanism - cutaneous vasodilatation that favors heat loss [17-21]. In the nausea/dizziness assay after provocative motion there is a decrease in head temperature and an increase in tail temperature. We have shown that in wildtype C57BL/6Jmice injection of Calcitonin Gene-Related Peptide (CGRP) prolongs this head temperature response and blunts the transient tail temperature increase, whereas a CGRP-receptor antagonist can reverse these CGRP-induced changes [22, 23] and Biorxiv doi.org/10.1101/2022.06.03.494762. Therefore, we investigated if a MA10-SARS-CoV-2 viral infection would show similar acute dizziness/nausea responses as CGRP injection, and if antagonizing CGRP signaling could reduce these dizziness/nausea responses.

111 **Materials and Methods**

112 **Animals**

113 A total of 180 mice (120 M/60F) were used in these studies, either 129SvEv (Taconic
114 129SVE) or C57B6/J (JAX 0664) or αCGRP (-/-) null mice on a 129SvEv background. Prior to
115 SARS-CoV-2 infection, mice were bred and housed under a 12 to 12 day/night cycle at the
116 University of Rochester 's Vivarium under the care of the University of Rochester's Veterinary
117 Services personnel. Mice were implanted with transponder chips (Backagin Microchip FDX-B
118 ISO 11784/11785) to allow for blinded identification; and when relevant, implanted with pellets
119 containing placebo or olcegepant (BIBN4096, Tocris; 2 mg/kg/day/SQ; Innovative Research of
120 America, Inc.). After pretesting was performed, mice were transferred to Cornell's ABSL3
121 facility, and acclimated prior to virus infection and testing. All animal procedures were approved
122 both by the University of Rochester's and Cornell University's IACUC committees and
123 performed in accordance with NIH standards.

124

125 **Virus propagation**

126 Vero-E6 cells (obtained through BEI resources, NIAID, NIH, NR-53726) were cultured in
127 Eagle's Minimum Essential Medium (ATCC, #30-2003) supplemented with 10% (vol/vol) fetal
128 bovine serum (FBS) (Gibco, CA) and 1% penicillin-streptomycin (Pen-Strep, Life Technologies)
129 at 37°C in a 5% (vol/vol) CO_2 atmosphere. Viral stocks of mouse-adapted SARS-CoV-2 (MA10)
130 (obtained from the laboratory Dr. Ralph Baric) were propagated in Vero-E6 cells in 2% (vol/vol)
131 FBS and 1% penicillin-streptomycin at 37°C at a multiplicity of infection (MOI) of 0.1. Viral stock
132 titers were determined by $TCID_{50}$ analysis. Viral propagation involving live SARS-CoV-2 was
133 conducted in Biosafety level 3 (BSL3) facilities both at the University of Rochester and at
134 Cornell University.

135

136 **Animal Biosafety level 3 (ABSL3) facility and viral inoculations**

137 Mice were anesthetized using isoflurane and subsequently intranasally infected with MA-
138 10 SARS-CoV-2. For infection with live virus, drops of the pre-characterized viral stock were
139 administered into the rostral meatus of the nose, with a total volume of 50 µL per mouse. Daily
140 monitoring and weighing of the mice were conducted until they reached a predetermined
141 humane endpoint of 20% weight loss from their starting weight and/or severe clinical signs, at
142 which point animals were humanely euthanized. Mouse studies were conducted in a BSL-3
143 laboratory and in accordance with protocols approved by the Institutional Animal Care and Use
144 Committee at Cornell University (IACUC mouse protocol # 2017-0108 and BSL3 IBC # MUA-
145 16371-1). See Fig. 1A.

146

147 **Motion-Induced Thermoregulation Testing**

148 Tu et al. first noticed thermoregulatory changes in the temperatures of the heads,
149 bodies, and tails of mice, in response to provocative motion [17] . We therefore adapted
150 their protocol for the present study (Biorxiv doi.org/10.1101/2022.06.03.494762). Head and
151 tail temperatures of C57B6/J mice were measured for a total of 45 minutes using a FLIR E60 IR
152 camera (model: E64501), as depicted in Fig. 1A. This camera was connected to a tripod and
153 positioned approximately 43 cm above an open, plexiglass box (mouse box) used to house an
154 individual mouse during testing. Both the tripod and mouse box were securely attached to the
155 shaker's base. Briefly, baseline measurements were recorded for five minutes prior to the
156 provocative motion (-5 to 0 mins). The provocative motion was an orbital rotation (75 rpm, 2-cm
157 orbital displacement), and mice were video-recorded for 20 minutes (0 to 20 mins). After 20
158 minutes, the provocative motion was turned off, and mice were video-recorded for an additional
159 20 minutes to measure recovery to baseline (20 to 40 mins) as schematized in Figs. 1A and 2.
160 Head and tail temperatures were measured after data retrieval using the software FLIR Tools+.
161 Tail and head temperatures were measured within predefined field of views: square region (3x3

162 mm) for tail, and circular region (10x10 mm) for head. Tail measurements occurred 2 cm from
163 the base of the tail and head measurements occurred at the center of the head image, in
164 between the mouse's ears. Infrared imaging data was collected every minute during baseline
165 measurements, and every 2 minutes during and after the provocative motion. We quantified
166 thermoregulatory changes to provocative motion by comparing changes in tail vasodilatations,
167 and we approximated the magnitude of the head hypothermia based on second order curve fit
168 estimates. Transient increases in the tail temperature of the mouse to provocative motion are
169 referred to as Δ *tail vasodilatations* (^{o}C), and were computed by subtracting the tail temperature
170 at time t = 0 minutes (rotation ON) from the max tail temperature measured during the first 10
171 mins of the rotation ($0 \leq t \leq 10$).

172

173 **Pulse Oximetry**

174 A mouse Stat Jr X (Kent Scientific) was used to measure oxygen saturation (O2%) of
175 mice (see Fig. 1B). The O_2 sensor was applied to the rear leg, and data were recorded following
176 readout stabilization, defined as an unchanging recording over 5 seconds.

177

178 **BAL harvest and tissue processing**

179 Mice were euthanized with CO_2, and bronco-alveolar lavage BAL fluid was removed
180 from the lung; animals then underwent laparotomy and sternotomy with subsequent left and
181 right ventricular cardiac perfusion with 20 mL total of PBS. Lungs were treated with 4%
182 paraformaldehyde/PBS (volume/volume) for a minimum of 72 hours to ensure full viral
183 inactivation. Tissues were taken out of the BSL3 facility and underwent dehydration with ethanol
184 and were later embedded in paraffin blocks for histological analysis.

185

186 **Histopathology**

187 For histological examination, mouse lungs were collected directly after euthanasia and
188 placed in 10% neutral buffered formalin for 72 h, after which tissues were embedded in paraffin.
189 Four-micrometer tissue sections were stained with hematoxylin for analysis.
190 Immunohistochemistry and digital image analysis for SARS-CoV-2 nucleocapsid was performed
191 as previously described [24]. Briefly, 4 μm tissue sections were labeled with a rabbit IgG
192 monoclonal antibody against SARS-CoV-2 nucleocapsid protein (GeneTex; GTX635679) at a
193 1:5,000 dilution and processed using a Leica Bond Max automated IHC Stainer. Digital image
194 analysis was performed using QuPath software v.0.2.3 [24-27].

195

196 **Imaging**

197 Histological specimens were visualized using a Zeiss Axioplan 2 microscope.
198 Immunohistochemistry (IHC) and hematoxylin and eosin (HE) stained slides for each specimen
199 were photographed in sequential order. In Adobe Photoshop, all images were sized with a
200 2080x2080 pixel frame and cropped to a uniform resolution of 1500x1500 pixels. IHC images
201 were further analyzed using Color Selection and Magic Wand tools where areas containing
202 brown staining were manually selected and cut into a separate layer. All images were exported
203 into JPEG format. For staining percentages, quantification was performed using ImageJ.
204 Images were converted from RGB Color into 8-bit grayscale and made Binary to set an
205 automated threshold. Area was then calculated with the Analyze Particles function. Circularity of
206 staining was assessed using the Circularity parameter set to 0.9-1.0.

207 **Quantification of lavage cytokines by ELISA**

208 Immulux 4HBx plates (ThermoFisher Scientific, #3855) were coated with IL-6 capture
209 antibody (ThermoFisher Scientific, MP5-20F3) and left overnight at 4°C. Wells were washed five
210 times with PBS+0.05% Tween 20 and blocked with PBS+5% dry milk solution (Bio-Rad,

211 1706404) for 1 hour at room temperature. 50µL of lavage sample or standard (R&D systems,
212 406-ML-005/CF) was added to the blocked wells for 2 hours at room temperature. Bound
213 cytokine was detected using a biotinylated IL-6 detection antibody (ThermoFisher Scientific,
214 MP5-32C11), streptavidin horseradish peroxidase (strep-HRP), and tetramethylbenzidine (TMB)
215 (ThermoFisher Scientific, 34028). Wells were washed three times following the addition of
216 detection antibody and strep-HRP. Reactions were stopped with 2N H_2SO_4 and ODs were read
217 at 450nm. Cytokine concentrations for each sample were determined by plotting OD values on a
218 standard curve using IL-6 recombinant protein. All testing was performed in triplicate.

219

220 **Statistics**

221 Two-way mixed effects (ME) models were used to assess % weight loss, and core
222 temperatures (^{o}C) across the factors: i) placebo vs olcegepant protection and ii) dpi. Two-way
223 ME models were also used to assess: i) viral infection vs pretest and ii) placebo vs olcegepant
224 protection for tail vasodilation responses at 3 dpi. Bonferroni multiple comparisons test was the
225 preferred post-hoc analysis method. X-intercept analyses of head recovery (mins) were
226 conducted assuming a quadratic model, least squares regression fitting, and constraints where
227 the x-intercept must be greater than x = 20 mins and the curve fit was approximated to x = 50
228 mins. Nested 1-way ANOVAs with Tukey post hoc was used to analyze BAL IL-6
229 concentrations and H&E staining (positive SARS-CoV-2 cells per mm^2).

230

231

232 **Results**

233 **MA-10 SARS-CoV-2 infection induces a fever-like state and disrupts**
234 **thermoregulation to provocative motion.** We measured baseline head temperatures in 18
235 month-old male /6J, 129SvEv, and 129 αCGRP-null groups of mice during pretesting and 3
236 days post-infection (dpi) with 10^5 pfu of MA-10 SARS-CoV-2 virus (**Fig. 2A&B**). Our results

237 showed a higher head temperature at 3 dpi, indicating a fever in all mice, regardless of strain
238 and olcegepant pretreatment (**Fig. 2B**).

239 We also measured motion-induced thermoregulation and weight changes in 18 month-
240 old male C57BL/6J, 129SvEv, and 129 αCGRP-null groups of mice at 3 dpi with 10^5 pfu of MA-
241 10 SARS-CoV-2 virus (**Fig. 3A**). Motion-induced thermoregulation was pre-tested in each
242 mouse 5-7 days prior to the infection. During the pre-test, we observed transient tail vasodilation
243 in response to provocative, nauseating stimuli (**Fig 3B,C,D**). The assay involved a 5-minute
244 baseline recording, a 20-minute rotation period (75 rpm, 1 cm orbital displacement), and a 20-
245 minute recovery period (as shown in **Figs. 1B and 3A**). Tail temperature profiles also indicated
246 a fever-like state after infection with MA-10 SARS-CoV-2, with higher tail temperatures at all
247 time points during the 3 dpi test than during the pretest (**Fig. 3B,C,D**). We computed a shift in
248 the Δ tail vasodilations by subtracting the magnitude of Δ tail vasodilations at 3 dpi from an
249 animal's pretest Δ tail vasodilation. With the exception of infected αCGRP-null mice, we
250 observed a decrease in the magnitude of tail vasodilations in infected mice compared to their
251 pretest, as indicated by a negative change in the Δ tail vasodilation - which is a sign of less
252 severe dizziness.

253 Typically, a twenty-minute provocative rotation in mice causes observable hypothermia,
254 and an additional 20-minute recovery period is needed for the mice to recover to their baseline
255 head temperature. Interestingly, we observed that viral infection delayed this recovery period, as
256 seen in our raw data (**Fig. 3 E,F,G**). Using a second-order polynomial fit ($B_0 + B_1X + B_2X^2$), we
257 estimated the time required for the mice to recover back to their baseline head temperature by
258 interpolating a curve fit to t = 50 minutes (**Fig. 3H).** We then computed a Δ head recovery by
259 subtracting the recovery period at 3 dpi from the pretest, where a positive Δ head recovery
260 indicated a longer recovery period due to the infection. In all infected males, regardless of
261 olcegepant treatment or strain, we observed a longer recovery period at 3 dpi ($p < 0.0001$). No

262 protective effects were seen by olcegepant in head temperature recovery for either strain (**Fig.**
263 **3H**).

264

265 **Olcegepant blockage or developmental loss of CGRP receptor leads to reduced IL-6**
266 **production in response to MA-10 infection**

267 SARS-CoV-2 infected 129/SvEv mice treated with olcegepant pellets had lower
268 interleukin 6 (IL-6) concentrations in their bronchoalveolar lavage (BAL) as compared to mice
269 treated with placebo (**Fig. 4B**). Congruently, the lower IL-6 concentrations in olcegepant-treated
270 mice were similar to the IL-6 concentrations measured in the αCGRP-null (-/-) mice (**Fig 4B**),
271 which is consistent with the relationship between CGRP and IL-6 levels in migraines [28]. In
272 C57BL/6J mice, similar observations regarding olcegepant's effects in reducing IL-6 post-
273 infection were observed but did not reach statistical significance (**Fig 4A**).

274 **Older mice treated with olcegepant recovered from the initial weight loss by 7 dpi.**

275 When 18-month-old C57 or 129S mice were infected with MA-10, those pretreated with
276 olcegepant pellets showed a faster recovery to baseline weight compared to mice that received
277 placebo pellets. This effect was observed in both female and male C57BL/6J mice (**Fig. 5A**), as
278 well as in older female and male 129SvEv mice (**Fig. 5B**). Notably, 129S αCGRP (-/-) null mice
279 of either sex experienced similar trends as 129S WT mice given olcegepant (**Fig. 5E**). Older
280 infected mice exhibited lower core temperatures compared to the uninfected groups; however,
281 olcegepant had no distinguishable effect on core temperatures regardless of age or strain (**Fig.**
282 **5 B,D,F**). In addition, MA-10 infection did not significantly impact O_2% saturation in mice
283 regardless of age, sex, or strain. However αCGRP-null mice exhibited lower weight loss trends
284 following virus infection that did WT mice - suggesting that the αCGRP-null mice have a
285 reduced sensitivity to the MA-10 virus.

286 Histological analysis of lung tissue revealed no significant differences in the number of
287 SARS-CoV-2 infected cells in the lungs of C57BL/6J or 129S WT mice at 3 dpi (**Fig. 6 A&B**).
288 However, olcegepant-protected mice and αCGRP-null mice showed reduced staining for SARS-
289 CoV-2 when compared to placebo-treated mice, and this observation correlated with IL-6 levels.
290 **Fig. 6 C&D** shows SARS-CoV-2 staining (scale = 100 μm) of C57BL/6J (**C**) and 129S (**D**) lung
291 tissues.

292

293

294 **Discussion:**

295 Early in the pandemic, there was a controversy as to whether CGRP plasma levels were
296 increased or decreased in COVID-19 disease [29, 30]. However, a recent study with a relatively
297 greater number of patients showed that elevated CGRP plasma levels are correlated with
298 increased disease severity in hospitalized COVID-19 patients [31]. In our study, the migraine
299 drug olcegepant (small molecule CGRP receptor antagonist) reduced IL-6 release at three days
300 post-infection (3 dpi) in two distinct wildtype mouse strains (C57B6 and 129S). Interestingly
301 however, there was not a similar protective effect on fever or on the dizziness/nausea-like state
302 elicited by SARS-CoV-2 MA-10 in these same infected mice, as tested at 3 dpi. However, we
303 did replicate in the mouse model both the fever and vestibular symptoms observed in COVID
304 patients [32, 33].

305 A few studies have investigated CGRP antagonism on individuals infected with SARS-
306 CoV-2. In one study [34], no deleterious effects of CGRP antagonism were found, and no
307 differences in symptom severity were found between CGRP antagonism to other treatment
308 modalities in migraine subjects. However, in this study, patients were not stratified by age. We
309 observed CGRP antagonism was protective from weight loss and IL-6 release only in older
310 mice. COVID-19 symptoms are more severe and mortality rates are higher in aged human
311 patients, adding significance to our results. Further, two relatively recent case studies showed
312 that increased headaches after SARS-CoV-2 infection can be treated with CGRP monoclonal
313 antibodies [35, 36]. Our study suggests that olcegepant or other CGRP treatments may be
314 further explored particularly to treat headaches or migraines in aged individuals and/or those
315 with high IL-6 levels upon COVID-19 infection.

316 In conclusion, in addition to the acute effects studied here, antagonizing CGRP signaling
317 may be therapeutic against long COVID, as long COVID patients also show higher IL-6 plasma
318 levels [37]. As long COVID has been demonstrated in mouse models [38], future plans include

319 investigating if antagonizing CGRP signaling in preclinical models can mitigate associated

320 neurological symptoms of long COVID [39].

321

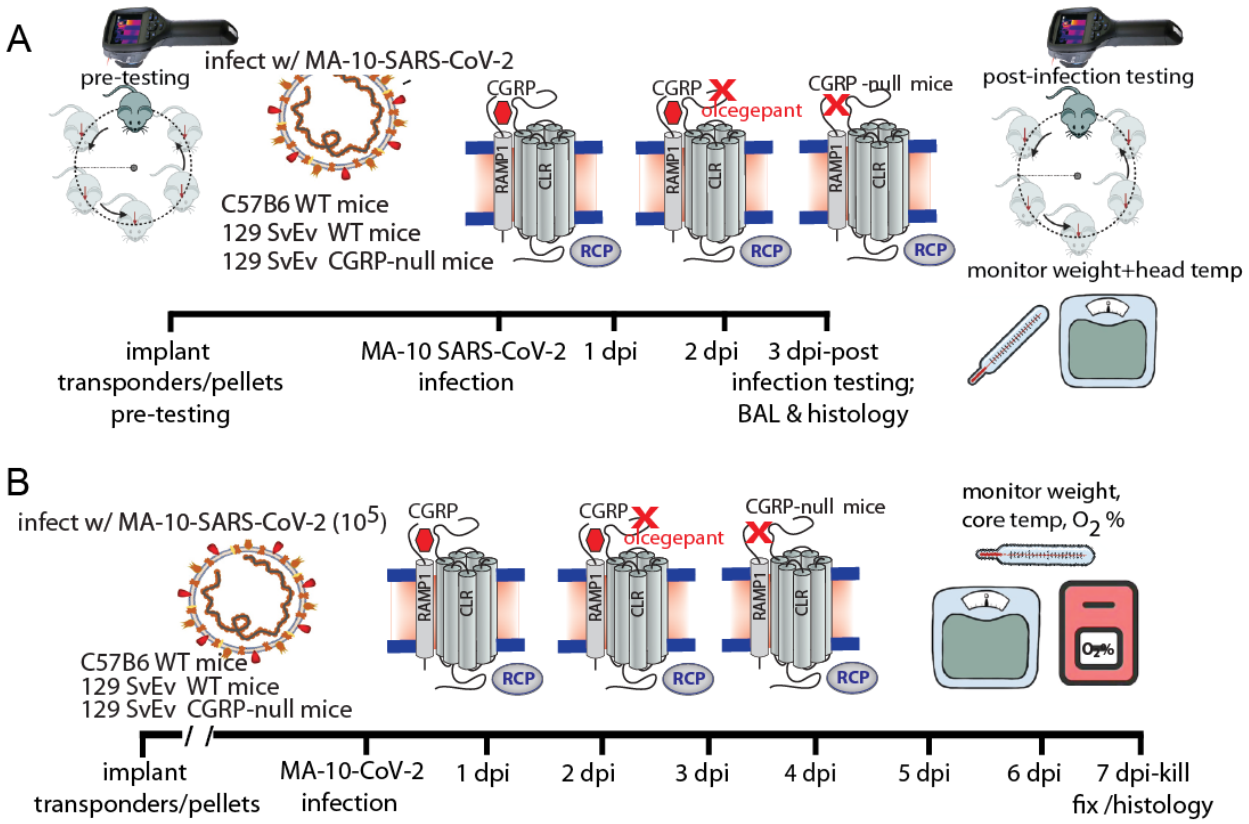
A
pre-testing
infect w/ MA-10-SARS-CoV-2
C57B6 WT mice
129 SvEv WT mice
129 SvEv CGRP-null mice
CGRP
RAMP1
CLR
RCP
olcegepant
CGRP -null mice
post-infection testing
monitor weight+head temp
implant transponders/pellets pre-testing
MA-10 SARS-CoV-2 infection
1 dpi
2 dpi
3 dpi-post infection testing; BAL & histology
B
infect w/ MA-10-SARS-CoV-2 (10^5)
C57B6 WT mice
129 SvEv WT mice
129 SvEv CGRP-null mice
CGRP
olcegepant
CGRP-null mice
monitor weight, core temp, O2 %
O2%
implant transponders/pellets
MA-10-CoV-2 infection
1 dpi
2 dpi
3 dpi
4 dpi
5 dpi
6 dpi
7 dpi-kill fix /histology

Fig. 1

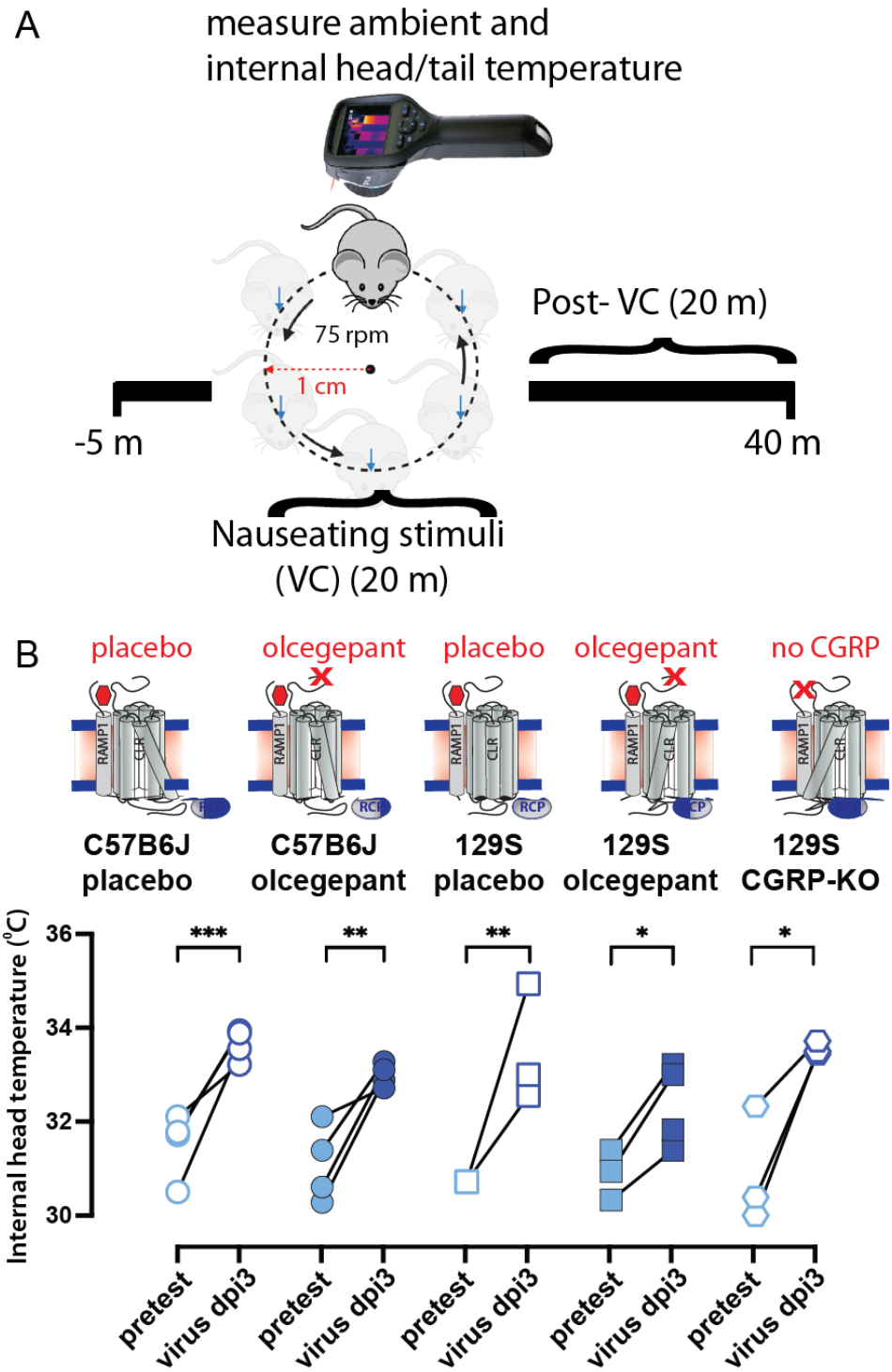
A
measure ambient and
internal head/tail temperature
75 rpm
1 cm
-5 m
Post- VC (20 m)
40 m
Nauseating stimuli
(VC) (20 m)
B
placebo
olcegepant
placebo
olcegepant
no CGRP
RAMP1
CLR
RCP
C57B6J
placebo
C57B6J
olcegepant
129S
placebo
129S
olcegepant
129S
CGRP-KO
Internal head temperature (°C)
36
34
32
30
***
**
**
*
*
pretest
virus dpi3

Fig. 2

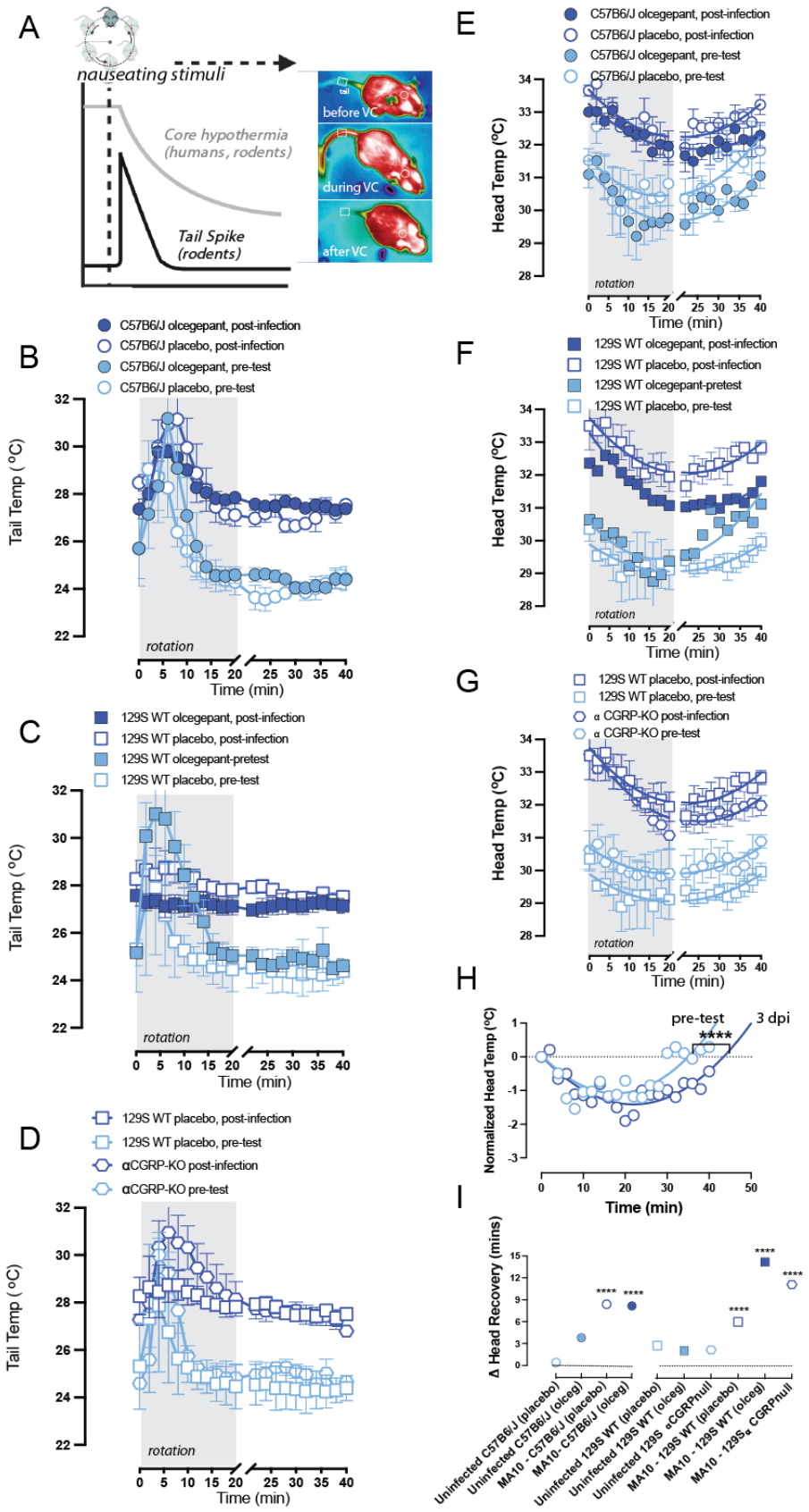
A
nauseating stimuli
Core hypothermia
(humans, rodents)
Tail Spike
(rodents)
tail
before VC
during VC
after VC
B
C57B6/J olcegepant, post-infection
C57B6/J placebo, post-infection
C57B6/J olcegepant, pre-test
C57B6/J placebo, pre-test
Tail Temp (°C)
rotation
Time (min)
C
129S WT olcegepant, post-infection
129S WT placebo, post-infection
129S WT olcegepant-pretest
129S WT placebo, pre-test
Tail Temp (°C)
rotation
Time (min)
D
129S WT placebo, post-infection
129S WT placebo, pre-test
αCGRP-KO post-infection
αCGRP-KO pre-test
Tail Temp (°C)
rotation
Time (min)
E
C57B6/J olcegepant, post-infection
C57B6/J placebo, post-infection
C57B6/J olcegepant, pre-test
C57B6/J placebo, pre-test
Head Temp (°C)
rotation
Time (min)
F
129S WT olcegepant, post-infection
129S WT placebo, post-infection
129S WT olcegepant-pretest
129S WT placebo, pre-test
Head Temp (°C)
rotation
Time (min)
G
129S WT placebo, post-infection
129S WT placebo, pre-test
α CGRP-KO post-infection
α CGRP-KO pre-test
Head Temp (°C)
rotation
Time (min)
H
pre-test
3 dpi
****
Normalized Head Temp (°C)
Time (min)
I
Δ Head Recovery (mins)
****
Uninfected C57B6/J (placebo)
Uninfected C57B6/J (olceg)
MA10 - C57B6/J (placebo)
MA10- C57B6/J (olceg)
Uninfected 129S WT (placebo)
Uninfected 129S WT (olceg)
Uninfected 129S αCGRPnull
MA10 - 129S WT (placebo)
MA10 - 129S WT (olceg)
MA10 - 129Sα CGRPnull

Fig. 3

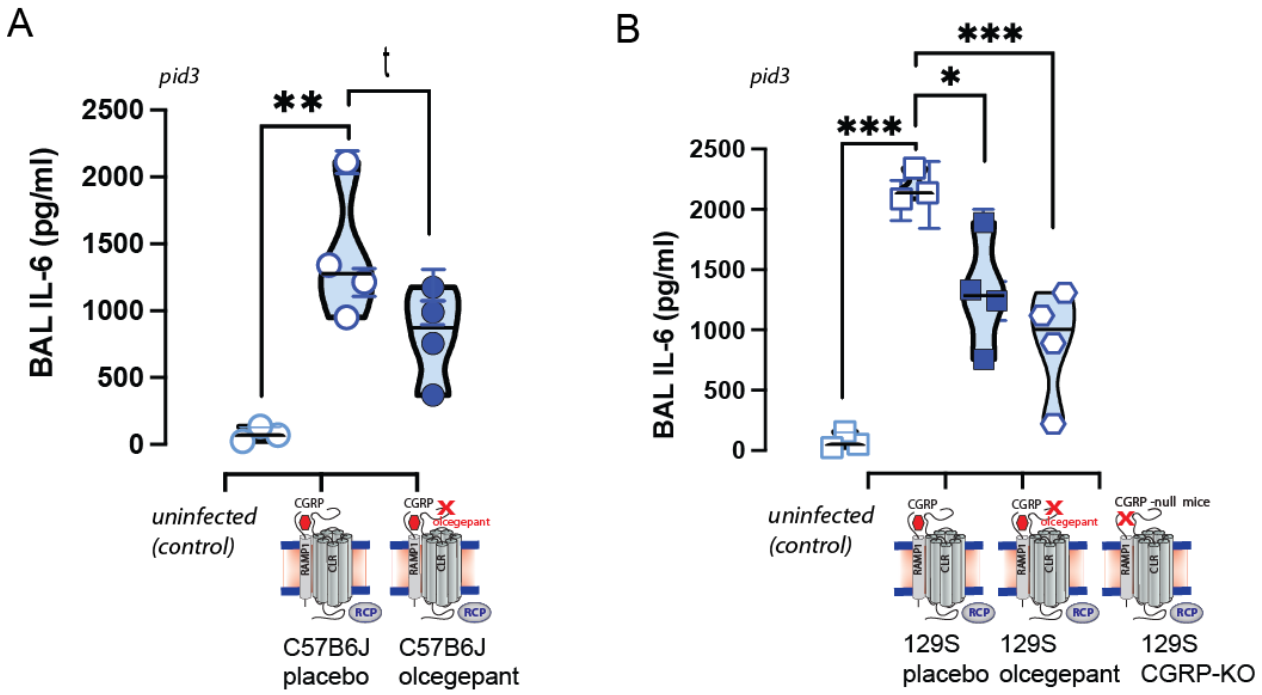
A
pid3
BAL IL-6 (pg/ml)
2500
2000
1500
1000
500
0
**
t
uninfected
(control)
CGRP
RAMP1
CLR
RCP
olcegepant
C57B6J
placebo
C57B6J
olcegepant
B
pid3
***
*
***
BAL IL-6 (pg/ml)
2500
2000
1500
1000
500
0
uninfected
(control)
CGRP
RAMP1
CLR
RCP
olcegepant
CGRP -null mice
129S
placebo
129S
olcegepant
129S
CGRP-KO

Fig. 4

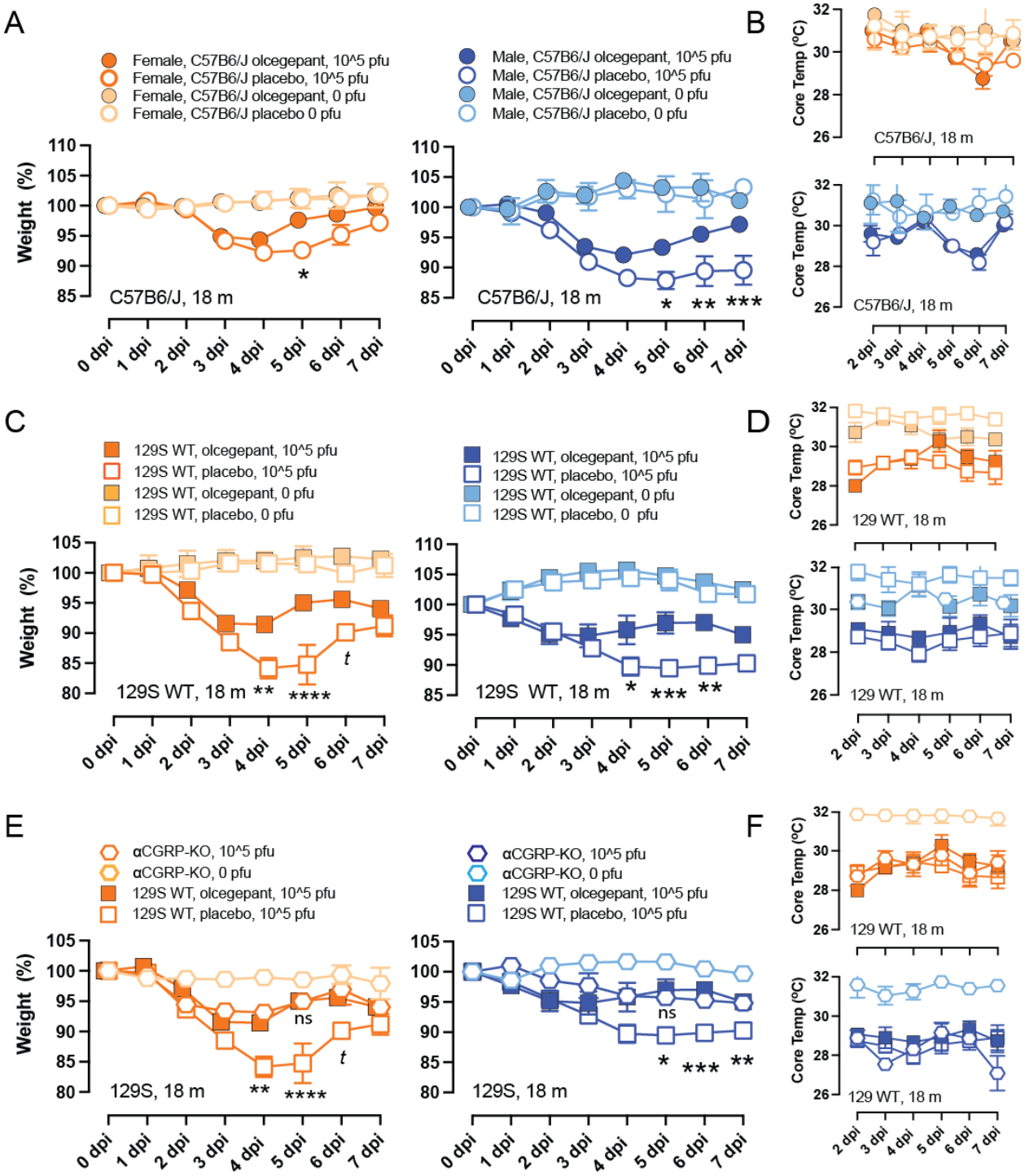
A
Female, C57B6/J olcegepant, 10^5 pfu
Female, C57B6/J placebo, 10^5 pfu
Female, C57B6/J olcegepant, 0 pfu
Female, C57B6/J placebo 0 pfu
Male, C57B6/J olcegepant, 10^5 pfu
Male, C57B6/J placebo, 10^5 pfu
Male, C57B6/J olcegepant, 0 pfu
Male, C57B6/J placebo, 0 pfu
Weight (%)
C57B6/J, 18 m
B
Core Temp (ºC)
C57B6/J, 18 m
C
129S WT, olcegepant, 10^5 pfu
129S WT, placebo, 10^5 pfu
129S WT, olcegepant, 0 pfu
129S WT, placebo, 0 pfu
129S WT, 18 m
D
129 WT, 18 m
E
αCGRP-KO, 10^5 pfu
αCGRP-KO, 0 pfu
129S WT, olcegepant, 10^5 pfu
129S WT, placebo, 10^5 pfu
129S, 18 m
ns
F
0 dpi
1 dpi
2 dpi
3 dpi
4 dpi
5 dpi
6 dpi
7 dpi

Fig. 5

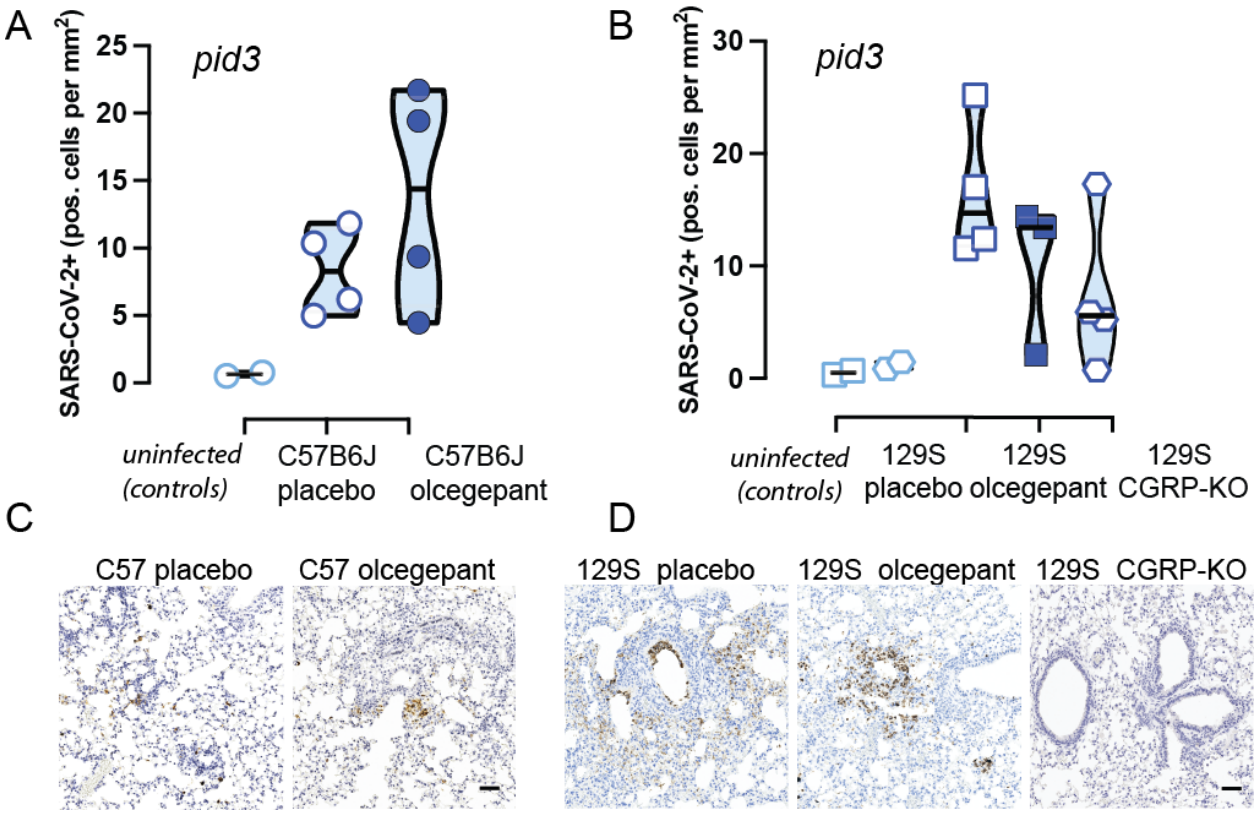
A
pid3
SARS-CoV-2+ (pos. cells per mm²)
25
20
15
10
5
0
uninfected (controls)
C57B6J placebo
C57B6J olcegepant
B
pid3
SARS-CoV-2+ (pos. cells per mm²)
30
20
10
0
uninfected (controls)
129S placebo
129S olcegepant
129S CGRP-KO
C
C57 placebo
C57 olcegepant
D
129S placebo
129S olcegepant
129S CGRP-KO

Fig. 6

357 **Figure Legends:**

358 **Fig. 1.** The study timelines are depicted. **A.** WT mice were infected with 10^5 pfu of MA-10
359 SARS-CoV-2 in the presence of placebo or CGRP-receptor antagonist olcegepant slow-release
360 pellets (olcegepant, BIBN4096, Tocris; 2 mg/kg/day/SQ) or mice lacking CGRP were infected
361 with the same virus; animals were then assessed for motion-induced nausea (dizziness) at 3
362 days after viral infection (dpi). At the completion of the nausea testing at 3dpi, bronchoalveolar
363 lavage (BAL) samples were collected for ELISA and lung tissue was obtained from control and
364 virus-infected animals at 3 dpi. Nausea (dizziness) was assessed for 45 minutes when mouse
365 was subjected to an orbital motion, noting temperature profiles (head and tail). **B.** WT mice
366 were infected with 10^5 pfu of MA-10 SARS-CoV-2 in the presence of placebo or CGRP-receptor
367 antagonist olcegepant slow-release pellets (olcegepant, BIBN4096, Tocris; 2 mg/kg/day/SQ) or
368 mice lacking CGRP were infected with the same virus; animals were then monitored for
369 changed in weight, core temperature and oxygen (O_2) saturation from 0 to 7 dpi.

370

371 **Fig. 2.** As shown in the **Fig 1A** timeline, older C57B/6, 129SvEv, and 129 mice lacking CGRP
372 were assessed for nausea (dizziness) when subjected to an orbital rotation, noting temperature
373 profiles (head and tail). **A.** Head and tail temperatures of mice were measured for a total 45
374 minutes using a FLIR E60 IR camera (model: E64501). This camera was connected to a tripod
375 and positioned approximately 43 cm above an open, plexiglass box (mouse box) used to house
376 an individual mouse during testing. Both the tripod and mouse box are securely attached to the
377 shaker's base. Briefly, baseline measurements were recorded for five minutes prior to the
378 provocative motion (-5 to 0 mins). The provocative motion was an orbital rotation (75 rpm, 2-cm
379 orbital displacement), and mice were recorded for 20 minutes (0 to 20 mins). After 20 minutes,
380 the provocative motion was turned off, and mice were recorded for an additional 20 minutes to
381 measure recovery to baseline (20 to 40 mins). Three mouse strains were tested: C57/B6J WT,
382 129S WT, and 129S αCGRP-null mice. Within each wild type (WT) strain, four groups of mice

383 were tested: placebo only, olcegepant only, placebo with 10^5 MA-SARS-CoV-2, and olcegepant
384 with 10^5 SARS-CoV-2 MA-10. Virus-infected mice were tested at Cornell University's ABSL-3
385 environment, with all pre-infection testing performed at University of Rochester. **B.** All tested
386 mice experienced a fever-like state 3 days post-viral infection (3 dpi). Olcegepant did not have a
387 protective effect in reducing this acute fever-like state at 3 dpi.

388

389 **Fig. 3. A.** Upon provocative motion, humans and mice will show a drop in head temperature
390 that recovers once rotation is ceased, and mice show a transient tail spike ~10 min into rotation.
391 When nausea or dizziness is present, the head temperature drop takes longer to recover, and
392 the transient tail spike diminishes or disappears. **B,C,D.** Viral infection diminishes tail
393 vasodilatations and impairs a mouse's natural response to the provocative motion. At time t = 0,
394 mice experience a 20-minute provocative motion and exhibit a significant increase in tail
395 temperature. Δ tails are computed and are corrected for ambient temperature. Findings suggest
396 that olcegepant did not protect against virus-induced changes in tail vasodilation at 3 dpi in all of
397 the strains tested. **E,F,G.** Viral infection impacts recovery from hypothermia after provocative
398 motion. **H.** Second order curve fits observed recovery of head temperatures after provocative
399 motion to baseline. Across all strains, mice experienced delayed temperature recovery
400 compared to pretest, with longer recovery profiles. **I.** No protective effects were seen by
401 olcegepant in temperature recovery for any of the tested strains.

402

403

404 **Fig. 4.** Bronco-alveolar lavage (BAL) samples were obtained for ELISA testing, and lungs were
405 obtained for subsequent immunohistochemistry at 3 dpi. MA-SARS-CoV-2 infection increased
406 the release of the inflammatory cytokine IL-6, and this IL-6 release was attenuated by CGRP
407 signaling blockade. In both C57B6/J **(A)** and 129S mice **(B)** strains, IL-6 release was

408 attenuated by olcegepant SQ release. Moreover, in αCGRP null mice, IL-6 cytokine release was
409 statistically equivalent to non-infected controls **(B)**.
410
411 **Fig. 5.** Older (18 months) female and male mice were tested for weight loss and core
412 temperature drops after infection with MA-10 SARS-CoV-2, 10^5 pfu virus at 0-7 dpi. **A. C.** We
413 found that animals treated with olcegepant recovered from the initial weight loss, with male mice
414 showing increased protection. **A.** C57B6/J; **C.** 129S. **E.** Similar to the IL-6 findings (**Fig. 4**),
415 mice lacking the CGRP peptide were not significantly different from uninfected controls. **B, D,**
416 **F.** Viral infection caused core temperatures of mice to decrease, and this effect was unaltered
417 by olcegepant treatment.
418
419 **Fig. 6.** A**&B.** There was no statistically significant difference in the number of SARS-CoV-2
420 antigen-positive cells in the lungs of (**A, C**) C57/B6J or (**B, D**) 129 mice, between mice that
421 received placebo versus olcegepant pellets at 3 dpi. **C, D.** Representative SARS-CoV-2
422 immunostaining is shown for 3 dpi lung issues from C57B6/J (**C**), and 129S (**D**) mice. Scale bar
423 is 100 μm. (*= $p < 0.05$, ** =$p < 0.01$, ** *= $p < 0.001$, **** = $p < 0.0001$)
424

425 **References:**

426 1. Zhu N, Zhang D, Wang W, Li X, Yang B, Song J, et al. A Novel Coronavirus from
427 Patients with Pneumonia in China, 2019. N Engl J Med. 2020;382(8):727-33. Epub 2020/01/25.
428 doi: 10.1056/NEJMoa2001017. PubMed PMID: 31978945; PubMed Central PMCID:
429 PMCPMC7092803.

430 2. Robertson CE. Could CGRP antagonists be helpful in the fight against COVID-19?
431 Headache. 2020. Epub 2020/05/10. doi: 10.1111/head.13853. PubMed PMID: 32386433.

432 3. Assas BM, Miyan JA, Pennock JL. Cross-talk between neural and immune receptors
433 provides a potential mechanism of homeostatic regulation in the gut mucosa. Mucosal Immunol.
434 2014;7(6):1283-9. Epub 2014/09/04. doi: 10.1038/mi.2014.80. PubMed PMID: 25183366.

435 4. Assas BM, Pennock JI, Miyan JA. Calcitonin gene-related peptide is a key
436 neurotransmitter in the neuro-immune axis. Front Neurosci. 2014;8:23. Epub 2014/03/05. doi:
437 10.3389/fnins.2014.00023. PubMed PMID: 24592205; PubMed Central PMCID:
438 PMCPMC3924554.

439 5. Channappanavar R, Perlman S. Pathogenic human coronavirus infections: causes and
440 consequences of cytokine storm and immunopathology. Semin Immunopathol. 2017;39(5):529-
441 39. Epub 2017/05/04. doi: 10.1007/s00281-017-0629-x. PubMed PMID: 28466096; PubMed
442 Central PMCID: PMCPMC7079893.

443 6. Aghagoli G, Gallo Marin B, Katchur NJ, Chaves-Sell F, Asaad WF, Murphy SA.
444 Neurological Involvement in COVID-19 and Potential Mechanisms: A Review. Neurocrit Care.
445 2021;34(3):1062-71. Epub 2020/07/15. doi: 10.1007/s12028-020-01049-4. PubMed PMID:
446 32661794; PubMed Central PMCID: PMCPMC7358290.

447 7. Liu Y, Zhang C, Huang F, Yang Y, Wang F, Yuan J, et al. Elevated plasma levels of
448 selective cytokines in COVID-19 patients reflect viral load and lung injury. Natl Sci Rev.

449 2020;7(6):1003-11. Epub 2020/06/01. doi: 10.1093/nsr/nwaa037. PubMed PMID: 34676126;
450 PubMed Central PMCID: PMCPMC7107806.

451 8. Bohn MK, Hall A, Sepiashvili L, Jung B, Steele S, Adeli K. Pathophysiology of COVID-
452 19: Mechanisms Underlying Disease Severity and Progression. Physiology (Bethesda).
453 2020;35(5):288-301. Epub 2020/08/14. doi: 10.1152/physiol.00019.2020. PubMed PMID:
454 32783610; PubMed Central PMCID: PMCPMC7426542.

455 9. Saniasiaya J, Kulasegarah J. Dizziness and COVID-19. Ear Nose Throat J.
456 2021;100(1):29-30. Epub 2020/09/16. doi: 10.1177/0145561320959573. PubMed PMID:
457 32931322; PubMed Central PMCID: PMCPMC7492824.

458 10. Doyle MF. Central nervous system outcomes of COVID-19. Transl Res. 2022;241:41-51.
459 Epub 2021/10/04. doi: 10.1016/j.trsl.2021.09.002. PubMed PMID: 34601116; PubMed Central
460 PMCID: PMCPMC8482653.

461 11. Bolay H, Karadas O, Ozturk B, Sonkaya R, Tasdelen B, Bulut TDS, et al. HMGB1,
462 NLRP3, IL-6 and ACE2 levels are elevated in COVID-19 with headache: a window to the
463 infection-related headache mechanism. J Headache Pain. 2021;22(1):94. Epub 2021/08/14. doi:
464 10.1186/s10194-021-01306-7. PubMed PMID: 34384355; PubMed Central PMCID:
465 PMCPMC8358545.

466 12. Carpenter KC, Yang J, Xu JJ. Animal Models for the Study of Neurologic Manifestations
467 Of COVID-19. Comp Med. 2023;73(1):91-103. Epub 2023/02/07. doi: 10.30802/AALAS-CM-22-
468 000073. PubMed PMID: 36744556; PubMed Central PMCID: PMCPMC9948905.

469 13. Kuba K, Imai Y, Rao S, Gao H, Guo F, Guan B, et al. A crucial role of angiotensin
470 converting enzyme 2 (ACE2) in SARS coronavirus-induced lung injury. Nat Med.
471 2005;11(8):875-9. Epub 2005/07/12. doi: 10.1038/nm1267. PubMed PMID: 16007097; PubMed
472 Central PMCID: PMCPMC7095783.

473 14. Ziegler CGK, Allon SJ, Nyquist SK, Mbano IM, Miao VN, Tzouanas CN, et al. SARS-
474 CoV-2 Receptor ACE2 Is an Interferon-Stimulated Gene in Human Airway Epithelial Cells and Is
475 Detected in Specific Cell Subsets across Tissues. Cell. 2020. Epub 2020/05/16. doi:
476 10.1016/j.cell.2020.04.035. PubMed PMID: 32413319.

477 15. Dinnon KH, 3rd, Leist SR, Schafer A, Edwards CE, Martinez DR, Montgomery SA, et al.
478 A mouse-adapted model of SARS-CoV-2 to test COVID-19 countermeasures. Nature.
479 2020;586(7830):560-6. Epub 2020/08/28. doi: 10.1038/s41586-020-2708-8. PubMed PMID:
480 32854108; PubMed Central PMCID: PMCPMC8034761.

481 16. Dinnon KH, 3rd, Leist SR, Schafer A, Edwards CE, Martinez DR, Montgomery SA, et al.
482 Publisher Correction: A mouse-adapted model of SARS-CoV-2 to test COVID-19
483 countermeasures. Nature. 2021;590(7844):E22. Epub 2021/01/21. doi: 10.1038/s41586-020-
484 03107-5. PubMed PMID: 33469219.

485 17. Tu L, Poppi L, Rudd J, Cresswell ET, Smith DW, Brichta A, et al. Alpha-9 nicotinic
486 acetylcholine receptors mediate hypothermic responses elicited by provocative motion in mice.
487 Physiol Behav. 2017;174:114-9. doi: 10.1016/j.physbeh.2017.03.012. PubMed PMID:
488 28302571.

489 18. Del Vecchio F, Nalivaiko E, Cerri M, Luppi M, Amici R. Provocative motion causes fall in
490 brain temperature and affects sleep in rats. Exp Brain Res. 2014;232(8):2591-9. doi:
491 10.1007/s00221-014-3899-8. PubMed PMID: 24658633.

492 19. Mazloumi Gavgani A, Hodgson DM, Nalivaiko E. Effects of visual flow direction on signs
493 and symptoms of cybersickness. PLoS One. 2017;12(8):e0182790. doi:
494 10.1371/journal.pone.0182790. PubMed PMID: 28777827; PubMed Central PMCID:
495 PMCPMC5544223.

496 20. Ngampramuan S, Cerri M, Del Vecchio F, Corrigan JJ, Kamphee A, Dragic AS, et al.
497 Thermoregulatory correlates of nausea in rats and musk shrews. Oncotarget. 2014;5(6):1565-
498 75. doi: 10.18632/oncotarget.1732. PubMed PMID: 24728971; PubMed Central PMCID:
499 PMCPMC4039232.

500 21. Romano F, Caramia N, Straumann D, Nalivaiko E, Bertolini G. Cross-coupling vestibular
501 stimulation: motion sickness and the vestibulo-sympathetic reflex. J Neurol. 2017. doi:
502 10.1007/s00415-017-8496-x. PubMed PMID: 28455665.

503 22. Doods H, Hallermayer G, Wu D, Entzeroth M, Rudolf K, Engel W, et al. Pharmacological
504 profile of BIBN4096BS, the first selective small molecule CGRP antagonist. Br J Pharmacol.
505 2000;129(3):420-3. Epub 2000/03/11. doi: 10.1038/sj.bjp.0703110. PubMed PMID: 10711339;
506 PubMed Central PMCID: PMCPMC1571877.

507 23. Mallee JJ, Salvatore CA, LeBourdelles B, Oliver KR, Longmore J, Koblan KS, et al.
508 Receptor activity-modifying protein 1 determines the species selectivity of non-peptide CGRP
509 receptor antagonists. J Biol Chem. 2002;277(16):14294-8. Epub 2002/02/16. doi:
510 10.1074/jbc.M109661200. PubMed PMID: 11847213.

511 24. Shapira T, Monreal IA, Dion SP, Buchholz DW, Imbiakha B, Olmstead AD, et al.
512 A TMPRSS2 inhibitor acts as a pan-SARS-CoV-2 prophylactic and therapeutic. Nature.
513 2022;605(7909):340-8. Epub 2022/03/29. doi: 10.1038/s41586-022-04661-w. PubMed PMID:
514 35344983; PubMed Central PMCID: PMCPMC9095466 US10988505B2) that cover matriptase
515 and other type II transmembrane serine proteases inhibitors for treating and preventing viral
516 infections, respiratory disorders, inflammatory disorders, pain disorders, tissue disorders,
517 hyperproliferative disorders, and disorders associated with iron overload. The remaining authors
518 declare that they have no competing interests.

519 25. Achanta R, Shaji A, Smith K, Lucchi A, Fua P, Susstrunk S. SLIC superpixels compared
520 to state-of-the-art superpixel methods. IEEE Trans Pattern Anal Mach Intell. 2012;34(11):2274-
521 82. Epub 2012/05/30. doi: 10.1109/TPAMI.2012.120. PubMed PMID: 22641706.

522 26. Bankhead P, Loughrey MB, Fernandez JA, Dombrowski Y, McArt DG, Dunne PD, et al.
523 QuPath: Open source software for digital pathology image analysis. Sci Rep. 2017;7(1):16878.
524 Epub 2017/12/06. doi: 10.1038/s41598-017-17204-5. PubMed PMID: 29203879; PubMed
525 Central PMCID: PMCPMC5715110.

526 27. Shapira T, Monreal IA, Dion SP, Jager M, Desilets A, Olmstead AD, et al. A novel highly
527 potent inhibitor of TMPRSS2-like proteases blocks SARS-CoV-2 variants of concern and is
528 broadly protective against infection and mortality in mice. bioRxiv. 2021. Epub 2021/05/12. doi:
529 10.1101/2021.05.03.442520. PubMed PMID: 33972944; PubMed Central PMCID:
530 PMCPMC8109206.

531 28. Han D. Association of Serum Levels of Calcitonin Gene-related Peptide and Cytokines
532 during Migraine Attacks. Ann Indian Acad Neurol. 2019;22(3):277-81. Epub 2019/07/31. doi:
533 10.4103/aian.AIAN_371_18. PubMed PMID: 31359937; PubMed Central PMCID:
534 PMCPMC6613407.

535 29. Abobaker A, Darrat M. Letter to the Editor From Abobaker and Darrat: "Circulating
536 Levels of Calcitonin Gene-Related Peptide Are Lower in COVID-19 Patients". J Endocr Soc.
537 2021;5(10):bvab052. Epub 2021/08/17. doi: 10.1210/jendso/bvab052. PubMed PMID:
538 34396020; PubMed Central PMCID: PMCPMC8083661.

539 30. Ochoa-Callejero L, Garcia-Sanmartin J, Villoslada-Blanco P, Iniguez M, Perez-Matute P,
540 Pujadas E, et al. Response to Letter to the Editor from Abobaker and Darrat: "Circulating levels
541 of Calcitonin Gene-Related Peptide Are Lower in COVID-19 Patients". J Endocr Soc.

542 2021;5(10):bvab053. Epub 2021/08/17. doi: 10.1210/jendso/bvab053. PubMed PMID:
543 34396021; PubMed Central PMCID: PMCPMC8083267.

544 31. Rizzi M, Tonello S, Morani F, Rizzi E, Casciaro GF, Matino E, et al. CGRP Plasma
545 Levels Correlate with the Clinical Evolution and Prognosis of Hospitalized Acute COVID-19
546 Patients. Viruses. 2022;14(10). Epub 2022/10/28. doi: 10.3390/v14102123. PubMed PMID:
547 36298678; PubMed Central PMCID: PMCPMC9611580.

548 32. Aedo-Sanchez C, Gutierrez G, Aguilar-Vidal E. COVID-19 and Vestibular Symptoms and
549 Assessment: A Review. Audiol Neurootol. 2023:1-7. Epub 2023/09/14. doi: 10.1159/000533448.
550 PubMed PMID: 37703853.

551 33. Jeong M, Ocwieja KE, Han D, Wackym PA, Zhang Y, Brown A, et al. Direct SARS-CoV-
552 2 infection of the human inner ear may underlie COVID-19-associated audiovestibular
553 dysfunction. Commun Med (Lond). 2021;1(1):44. Epub 2021/12/07. doi: 10.1038/s43856-021-
554 00044-w. PubMed PMID: 34870285; PubMed Central PMCID: PMCPMC8633908.

555 34. Caronna E, Jose Gallardo V, Alpuente A, Torres-Ferrus M, Sanchez-Mateo NM,
556 Viguera-Romero J, et al. Safety of anti-CGRP monoclonal antibodies in patients with migraine
557 during the COVID-19 pandemic: Present and future implications. Neurologia (Engl Ed).
558 2021;36(8):611-7. Epub 2021/10/17. doi: 10.1016/j.nrleng.2021.03.005. PubMed PMID:
559 34654536; PubMed Central PMCID: PMCPMC8506139.

560 35. Grassini A, Marcinno A, Roveta F, Gallo E, Cermelli A, Boschi S, et al. Impact of COVID-
561 19 on chronic migraine treated with erenumab: a case report. Neurol Sci. 2021;42(8):3079-81.
562 Epub 2021/05/23. doi: 10.1007/s10072-021-05329-5. PubMed PMID: 34021438; PubMed
563 Central PMCID: PMCPMC8139216.

564 36. Ozkan E, Celebi O, Keskin O, Gursoy A, Gursoy-Ozdemir Y. Is Persistent Post-COVID
565 Headache Associated With Protein-Protein Interactions Between Antibodies Against Viral Spike

566 Protein and CGRP Receptor?: A Case Report. Front Pain Res (Lausanne). 2022;3:858709.
567 Epub 2022/04/19. doi: 10.3389/fpain.2022.858709. PubMed PMID: 35434707; PubMed Central
568 PMCID: PMCPMC9011137.

569 37. Littlefield KM, Watson RO, Schneider JM, Neff CP, Yamada E, Zhang M, et al. SARS-
570 CoV-2-specific T cells associate with inflammation and reduced lung function in pulmonary post-
571 acute sequalae of SARS-CoV-2. PLoS Pathog. 2022;18(5):e1010359. Epub 2022/05/27. doi:
572 10.1371/journal.ppat.1010359. PubMed PMID: 35617421; PubMed Central PMCID:
573 PMCPMC9176759.

574 38. Dinnon KH, Leist SR, Okuda K, Dang H, Fritch EJ, Gully KL, et al. A model of persistent
575 post SARS-CoV-2 induced lung disease for target identification and testing of therapeutic
576 strategies. bioRxiv. 2022. Epub 2022/02/24. doi: 10.1101/2022.02.15.480515. PubMed PMID:
577 35194605; PubMed Central PMCID: PMCPMC8863140.

578 39. Jansen EB, Orvold SN, Swan CL, Yourkowski A, Thivierge BM, Francis ME, et al. After
579 the virus has cleared-Can preclinical models be employed for Long COVID research? PLoS
580 Pathog. 2022;18(9):e1010741. Epub 2022/09/08. doi: 10.1371/journal.ppat.1010741. PubMed
581 PMID: 36070309; PubMed Central PMCID: PMCPMC9451097.
582